Biomimetic Flip-and-Flap Strategy of Flying Objects for Perching on Inclined Surfaces

Zhifeng Huang , Sen Li , Jungao Jiang, Ying Wu , Liang Yang, and Yun Zhang

Abstract—Animals can use the maneuver of a flipping body and flapping wings to reduce the normal rebound force of impact during landing, decreasing the adsorption force required by the contact point. This capability aids aerial vehicles with landing not only on vertical surfaces, but also on inclined surfaces. In this study, a "*flip-and-flap*" biomimetic strategy is presented that enables a high-speed flying object to perch on inclined surfaces without speed reduction before touchdown. During perching, the kinetic energy of the aerial vehicle is first converted to potential energy by flipping upward with a customized extended leg. Then, with a controlled thrust, the potential energy is consumed during the downward-swing phase. Thus, the aerial vehicle can land smoothly on a wall. Simplified and multilink models were designed to simulate the landing of a flying object, and the dynamic interaction between the flying object with an extended-leg mechanism and the surface was elaborated. A set of experiments on perching performed with the proposed strategy and customized extended leg, demonstrating the effectiveness and robustness of the strategy.

Index Terms—Biologically-inspired robots, aerial systems: mechanics and control, dynamics.

I. INTRODUCTION

IN THIS study, the feasibility of performing flip lands, a well-known attribute of a landing maneuver of the *Musca domestica* [1]-[4], through the operation of inertial dynamics while excluding speed-reducing before touchdown, was investigated. Some lower animals, such as *M. domestica*, have poor visual acuity, and *M. domestica* are clearly not intelligent enough to predict when to land. Thus, it is probably too late to slow down when landing, so they do so without deceleration. *M. domestica* have reflexes that are based on the nature and type of external stimuli. However, they are good at using their front legs and pulvilli for a large supination based on the type of external stimuli, which enables their landing to become more convenient, safe, and stable. In addition to *M.domestica*, bats [5]-[7] also
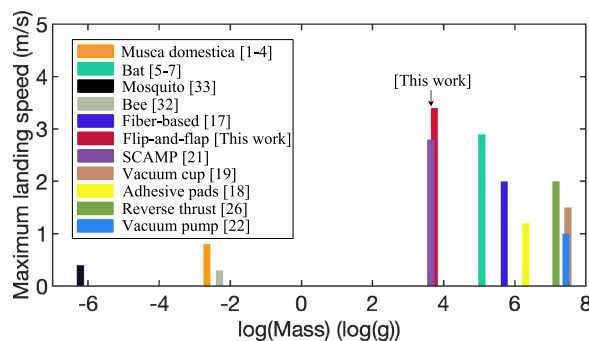
Fig. 1. Comparison chart of impact speed and mass for animals and robots. The height of the mark on the chart is their maximum landing speed, and the width of the mark on the chart is their log(mass).

utilize their wing inertia to perform complex body rolls, which act as a buffer which reduces the wall normal stress. Combined, the flipping body and flapping wings of animals reduce the impact force during landing and decrease the adhesion force required by the contact point. This strategy helps flying objects perch on platforms with varying tilt, increasing their operation time. This capability is particularly valuable for small aerial vehicles because smaller vehicles have less endurance. The applications of perching aerial vehicles are common in a wide range of surveillance and detection tasks. Perching on a wall surface enables the aerial vehicle to conserve energy rather than hovering following a disaster, such as an earthquake or during an inspection of remote buildings.

The present work, inspired by flying insects that land on near-vertical surfaces, builds on prior work on perching airplanes. The maneuvering of animal landings and the strategy of airplane perching have attracted relatively large number of studies [8]. Different body roll maneuvers were applied in the landing strategy of flying objects, such as pitch up, a direct approach, and upward flip. These strategies were achieved mainly by state estimation, control algorithms, and the attachment mechanism. The available performance data (maximum landing speed and mass) of each system are plotted as a single bar in Fig. 1.

Pitch-up maneuvers [9]-[16] focus on landing a flying object by deceleration under absolute situational awareness, which means the state of the flying vehicle is estimated by motion capture systems, computer vision, ranging sensors, or inertial measurement units (IMUs). Direct approach maneuvers [17]-[20] contribute to reducing the required situational awareness of the flying object, but the large pitch-back moment needs to be resolved. In some studies, upward-flip [21]-[22] maneuvers were performed by pivoting nose down into an inverted configuration. Additionally, there are perching methods focusing on inclined surfaces. In a previous study [23], a nonlinear
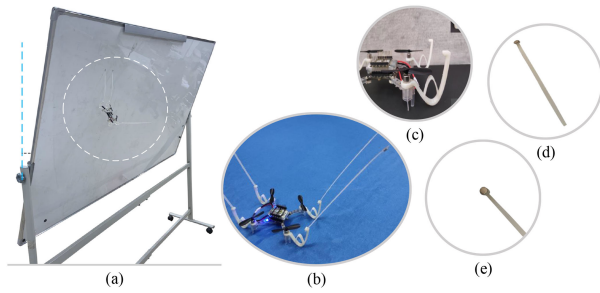
Fig. 2. (a) Whiteboard selected to act as vertical and inclined surfaces, (b) Crazyflie 2.0 quadrotor with extended-leg mechanism, (c) elastic thigh part, (d) 15-cm-long cable tie, and (e) adsorption part – a miniature magnet with a diameter of 5 mm and a thickness of 1.5 mm.

hybrid control method was used for landing on an unknown inclined surface at $30°$, but it required downward observation using lasers and a CMOS camera. In another study [24], a downward-facing strategy was developed by using multirotor agility to enable aerial vehicles to stick on inclined surfaces, but the strategy relied on an external motion capture system for absolute situational awareness. Researchers have also installed additional horizontal rotors to land at $30°$ inclinations [25]. Others [26] proposed that reverse thrust contributes to improving the multirotor drop landing performance at $25°$ inclinations, but it is only suitable for landing from top to bottom. Most of the proposed perching methods require deceleration beforehand, and landing on negatively inclined surfaces has seldom been considered. In other words, manual remote control or using sensors to estimate the distance between the wall and the vehicle is necessary. However, deceleration under state estimation in advance is not necessarily useful in a complex environment because a) motion capture systems are not necessarily applicable in an open outdoor environment, b) the performance of visual sensors is easily affected by occlusion and lighting conditions, and c) radar detection needs to avoid specular reflection. Thus, landing without deceleration would be valuable and deserves further study.

To improve the effectiveness and reliability of the perching strategy further, rather than relying on state estimation sensors, a method is proposed to supplement the previous method. An attempt was made to analyze in detail the body roll strategy, combining the upward flip with the downward swing to explore the possibility of landing on inclined surfaces without speed reduction before touchdown.

The upward-flip operation employs an extended-leg mechanism (Fig. 2b) to convert energy, and the downward-swing operation mimics a biological flapping motion by generating a controlled thrust to achieve a wall landing, aiming to land not only on vertical surfaces, but also on negatively inclined surfaces.

Fig. 3 shows the progress that simplified model of the biomimetic *flip-and-flap* strategy applied to a flying object with an extended leg. Initially, the flying object hits the wall surface with a certain amount of kinetic energy. At the impact moment, the extended leg helps the flying object pivot around the contact point and flip upward at the wall surface (the "flip" phase). After reaching the top, the flying object begins to swing downward using the controlled thrust of the propellers to consume the potential energy (Fig. 3 e) (the "flap" phase). The downward motion is called "flapping" because, in this process, the propeller and

the insect flutter wing have almost similar roles–both consume potential energy by generating a upward thrust [27]. Finally, stable landing is achieved using this *flip-and-flap* strategy, and the flying object can perch.

Details of the bionic structure (extended-leg mechanism) and experimental platform are discussed in the following section. The model of the biomimetic strategy for perching is discussed in Section III. In Section IV, the performance of the strategy according to the simulation is described. The experiments implemented are discussed in Section V. Finally, concluding remarks are made in Section VI.

II. EXPERIMENTAL PLATFORM

To verify the hypothesis that it is possible to perform flip landings, a biomimetic strategy was demonstrated by building the experimental platform described in this section.

A. Specifications of Flying Platform

The Crazyflie 2.0 (Fig. 2 b) quadrotor [28]-[29] was chosen as the experimental platform because it is common in the flying object area of research, and it fulfills the dynamic requirements. Crazyflie 2.0 is equipped with an IMU, the MPU-9250. The sensor contains a triaxial gyroscope and a triaxial accelerometer. The sampling frequency is up to 100 Hz and meets the requirements of real-time recording of quadrotor attitude changes during landing. The weight of the quadrotor is 32 g, and its moment of inertia is $I = diag[2.3951, 2.3951, 3.2347] \cdot 10^{-5} kg \cdot m^2$.

B. Extended Leg

The extended legs weigh 10 g in total, and they are attached to a 32 g Crazyflie quadrotor for a total robot weight of 42 g.

Each support foot of the quadrotor has an extended-leg mechanism. Each extended-leg mechanism consists of three parts: an elastic thigh part, a cable tie, and an adsorption part.

The elastic thigh acts as an insect's thigh to provide stiffness and damping and works during upward flipping. Each elastic thigh was fabricated from an elastomeric material, ABS, using a 3D printer. Its light weight (1.35 g), appropriate stiffness, and damping can effectively cushion the violent impact force at the moment of collision.

The cable tie acts as the insect's foreleg to provide a suitable moment arm during downward swing. Each elastic thigh corresponds to a cable tie. The end of the cable tie is mounted in the slot of the elastic thigh. Appropriate flexibility makes flying objects better suited to dealing with different surface inclinations. The experiments used a 15 cm-long and 0.9 g cable tie as flexible tissue to mimic a flexible foreleg.

The adsorption part acts as an insect's pulvilli to provide a small adsorption capacity to attach to the surface. To provide different inclinations ranging from $-90°$ to $90°$ (marked as α, shown in Fig. 2 a), an adjustable whiteboard was selected to act as the wall surface. Because of the magnetic properties of the whiteboard, the other end of the cable tie had a 0.25 g miniature magnet acting as pulvilli to provide an appropriate force of adsorption (approximately 1 N).

The selection of cable ties and magnets was determined by repeated experiments considering the stability of landing and ease of take-off (Table I). An excessively large magnetic force is not conducive to take-off, wheras too small a force is likely to cause the aircraft to break away from the wall in the process of
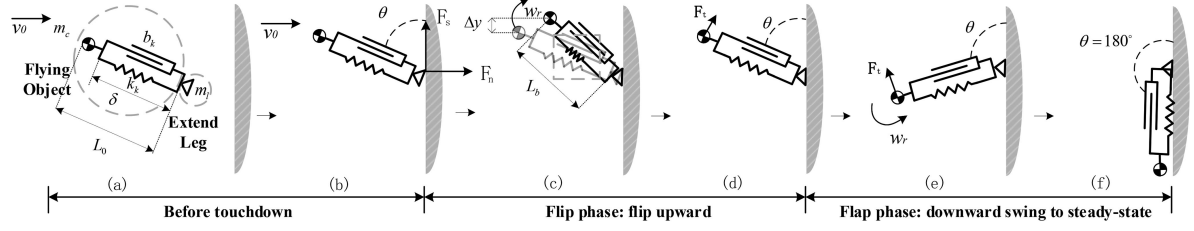
Fig. 3. Simplified model (left to right): Process of maneuver implemented on aerial object: (a) initial configuration with δ, (b) aerial object hits the wall, (c) aerial vehicle swings upward and reaches its maximum altitude, (d)-(e) downward swing under the controlled thrust F_t, while pitch angle θ and the pitch rate $\dot{\theta}$ are the control inputs, and (f) successful perching.

TABLE I
SELECTION OF CABLE LENGTH AND MAGNET SIZE

Length of Cable Tie (cm)	Size of Magnet (Diameter × Thickness) (mm)				
	3×1.5	4×1.5	$3\times1.5+2\times1$	5×1.5	$5\times1+3\times1$
9	+	−	−−	−−	−−
12	++	−	−−	−−	−−
15	++	++	++	+	−
18	++	++	++	+	−

[0]* Take-off ability: −−: Unable, −: Difficult, +: Acceptable, ++: Easy.

TABLE II
RELATED PARAMETERS OF SIMPLIFIED MODEL

Character	Definition
k_k, b_k	Spring stiffness (N/m), damping coefficient (N.s/m)
F_t	Resultant force of the thrust (N)
m_l, m_c	Extended leg mass (kg), flying object mass (kg)
I	Flying object mass moment of inertia
L_0	Initial length of the flying object (m)
L_b	Current length of the flying object (m)
$^b x$	Compression of spring (m)
v_0	Impact velocity (m/s)
v_v	Velocity component perpendicular to flying object (m/s)
θ_0	Initial angle between flying object and surface (rad)
θ	Current angle between flying object and surface (rad)
Q_b	Energy consumed by damper (J)
k_p, k_d	Gain P, gain D of PD controller (N/rad), (N.s/rad)

turning over. In addition, the longer the tie, the better the takeoff. However, owing to the centrifugal effect, a tie that is too long can easily cause the aircraft to break away from the wall during the swinging process.

III. MODEL

In this section, details of the simplified model and the multi-link model are presented. The related parameters of the simplified model are listed in Table II.

Fig. 3 shows the flying object attached to a spring with stiffness k_k and subject to damping coefficient b_k; b denotes the body frame of the flying object. The hypotheses for this simplified model are as follows: a) the damping force is proportional to the object velocity, b) m_l is much smaller than m_c, c) the compression of the spring is $^b x = L_0 - L_b$, and d) the wall friction is strong enough (after contact of the extended leg with the wall surface, the extended leg helps the flying object flip up at the fulcrum). The dynamics equation of this system is:

$$m_c(L_0 - {}^b x)\ddot{\theta} = m_c g \sin\theta - F_t \qquad (1)$$

$$m_c {}^b \ddot{x} = m_c g \cos\theta - k_k(L_0 - L_b) - b_k {}^b \dot{x} \qquad (2)$$

If b_k is a heavy damper, heavy damping results in the conversion of kinetic energy into thermal energy. Owing to the inertia of the flying object, the additional kinetic energy is converted into gravitational potential energy through flipping upward. Simultaneously, if the spring is weak (i.e., k_k is small), some kinetic energy is converted into spring potential energy. The spring acts as a buffer, and the stored energy is slowly released during the downward swing.

To separate the flip and flap phases, the center of mass (CoM) must meet two requirements simultaneously: a) the spring reaches the maximum compression, and b) the center of mass also reaches its maximum altitude. The state of the system can be called a "zero kinetic energy state" if it satisfies the above conditions. To achieve the zero kinetic energy state in the simplified model, the following condition should be satisfied:

$$\frac{d\theta}{dt} = 0, \quad \frac{d^b x}{dt} = 0 \qquad (3)$$

Under this premise, both the altitude and compression reached their maximum, which means that all kinetic energy decreased to zero – converted into potential energy.

A. Flip Phase: Impact and Upward-Flip in Simplified Model

Starting from a user-defined position, heading angle, and velocity, the flying object flies toward the wall surface. Subsequently, it impacts the wall with an initial kinetic energy. It is believed that the surface exerts a rebound force to push the flying object off the surface. Thus, a biomimetic strategy is required. Fig. 3 shows the progress of the biomimetic strategy applied to the flying object. At the moment of collision, the propeller is shut off (Fig. 3b). Fig. 3 c shows that the flying object flips up to reach its maximum altitude. The kinetic energy decreases when the CoM flips up because some energy is consumed by the damper and other energy is stored in gravitational potential energy and spring potential energy. When the flying object is in the zero kinetic energy state, its work–energy conversion can be expressed as follows:

$$\frac{1}{2}m_c v_0^2 = m_c g(L_0 \cos\theta - {}^b x \cos\theta - L_0 \cos\theta_0)$$
$$+ \frac{1}{2}k_k {}^{2b}x - \int_0^t b_k {}^b \dot{x}^2 dt \qquad (4)$$

It is assumed that the spring compression is less than 1%, thus there is almost no compression (i.e., heavy b_k) during the entire process. Therefore, $\frac{m_c v_v^2}{2}$ is considered that all energy is converted into gravitational potential energy. The work–energy conversion relationship can be simplified into the following
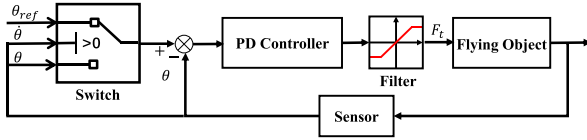
Fig. 4. Schematic of controller, where a) θ is the pitch angle of the flying object, b) θ_{ref} is a reference signal, c) the rate of the pitch angle $\dot{\theta}$ is used to trigger the controller, d) the filter is used to avoid numerical overflow.

equation when the flying object is in the zero kinetic energy state.

$$\frac{1}{2}m_c v_v^2 = m_c g(L_0 cos\theta_{min} - L_0 cos\theta_0) \tag{5}$$

where $v_v = v_0 cos\theta_0$.

Meanwhile, θ reaches its minimum, θ_{min}.

$$\theta_{min} = arccos\frac{\frac{1}{2}m_c v_v^2 - m_c g L_0 cos\theta_0}{m_c g L_0} \tag{6}$$

When the damper is sufficiently heavy, θ reaches its minimum. Otherwise, some energy from $\frac{1}{2}m_c v_v^2$ is converted to spring potential energy.

B. Flap Phase: Controlled Downward Swing in Simplified Model

After the flying object upward flip reaches the maximum altitude, the object performs a pendulum-like motion to a downward swing, as illustrated in Fig. 3e. However, if the swing is so violent that F_n increases beyond the adsorption capacity, the flying object detaches from the surface. Thus, the flying object in the pitch angle is adjusted by a PD controller to prohibit severe swing as θ reaches $180°$ (Fig. 3 f).

The motion of the object at this stage is analogous to a pendulum (the aerodynamic drag is assumed to be negligible). The dynamics equation of this system is:

$$I\ddot{\theta} = m_c g sin\theta L_b - F_t L_b \tag{7}$$

The normal rebound force F_n at the point of contact can be formulated as:

$$F_n = (F_t - m_c L_b \ddot{\theta})cos\theta + m_c \dot{\theta}^2 L_b sin\theta \tag{8}$$

The normal rebound force is the resultant force of the propeller thrust, centripetal force, and inertia force of the flying object. To prevent detachment of the extended leg and wall surface, this normal force must be as small as possible.

Hence, the force F_t of the propeller is used to decrease the normal rebound force during the downward swing. In addition, F_t is used to reduce the rotational velocity $\dot{\theta}$ and acceleration $\ddot{\theta}$ of the flying object using a pitch angle PD controller. The propeller thrust F_t is adjusted by the pitch controller, which is used to perch stably, prohibiting severe swing. Under pitch control, the velocity of the flying object quickly approaches zero. A schematic of the pitch PD controller is shown in Fig. 4.

Once the flying object impacts the wall surface, an automated routine detects the rotational velocity $\dot{\theta}$ to determine whether it is in the downward-swing phase. During the downward-swing phase, the rotational velocity is greater than zero ($\dot{\theta} > 0$), and the reference signal θ_{ref}, current pitch θ, and rate of the pitch $\dot{\theta}$ become the control input. Therefore, when this optimization

TABLE III
RELATED PARAMETERS OF MULTILINK MODEL

Character	Definition
F_t	Resultant force of the thrust (N)
θ	Current pitch angle of the flying object (rad)
(f_B, τ_B)	Force and moment on the body (except gravity)
$(\dot{v}_{oB}, \dot{\omega}_B)$	Spatial acceleration of the body
$u, \ddot{q}$	All joint torques, all joint accelerations
f_j	Force from body side (mother) to link j
τ_j	Moment from body side (mother) to link j
I_j^S	Spatial inertia matrix
ξ	Spatial velocity of a rigid body
f_{j+1}	Force reaction effect from the child link j+1
τ_{j+1}	Moment reaction effect from the child link j+1
f_j^E	The environmental force directory acting on link j
τ_j^E	The environmental moment directory acting on link j
k_i	Stiffness of elastic thigh part (N/rad)
b_i	Damping coefficient of elastic thigh part (N.s/rad)
K_n	P parameter of normal force (N/m)
D_n	D parameter of normal force (N.s/m)
h_f	Displacement of contact point
D_s	P parameter of shear force (N.s/m)

condition ($\dot{\theta} > 0$) is triggered, the PD controller is used to adjust the thrust.

C. Multilink Dynamics Mode

A multilink dynamics model was designed to simulate the landing of a flying object on surfaces during the entire landing process. Validation testing of the *flip-and-flap* method was performed in the simulation environment. The related parameters of the multilink model are shown in Table III.

The Newton–Euler method was used to establish the system dynamics equation of a multilink system, and the dynamics analysis in the collision and bounce-off phases was performed.

Given the input of the robot $u_G = [f_B \ \tau_B \ u]^T$, the acceleration $\ddot{x}_G = [\dot{v}_{oB} \ \dot{\omega}_B \ \ddot{q}]^T$ can be calculated as:

$$\ddot{x_G} = A_G^{-1}(u_G - b_G) \tag{9}$$

All components of the inertia matrix A_G and the vector b_G representing the Coriolis and centrifugal forces, and gravity can be calculated using the unit vector method [30].

A recurrence equation is used to give the propagation of the force and moment:

$$\begin{bmatrix} f_j \\ \tau_j \end{bmatrix} = I_j^S \dot{\xi}_j + \xi_j \times I_j^S \xi_j - \begin{bmatrix} f_j^E \\ \tau_j^E \end{bmatrix} + \begin{bmatrix} f_{j+1} \\ \tau_{j+1} \end{bmatrix} \tag{10}$$

During flight, the flying object is subjected to aerodynamic forces and gravity, and the propeller provides the thrust required for flight. The aerodynamic drag is assumed to be negligible. The model for the various forces is described as follows.

1) *Gravity:* The forces of gravity are applied at the center of mass of each body.
2) *Body Joints:* To simulate the elastic joint of the extended legs, a control force is applied to the joint by means of an impedance model to maintain elasticity. The vector of the joint torque τ_i can be expressed as an equation of joint stiffness, damping, and equilibrium position:

$$\tau_i = k_i(\theta_i - \theta_{i_0}) + b_i \dot{\theta}_i \tag{11}$$

The contact between the legs and the wall surface is modeled using a spring damper at each contact point. The contact model is described below.

k_k	b_k	Potential Energy(J)	Thermal Energy(J)
20	0	(0.027, 0.087)	0.000
15	0.4	(0.032, 0.045)	0.038
10	0.8	(0.035, 0.023)	0.058

* (gravitational potential energy, spring potential energy).

In the normal direction of the wall surface, the normal force F_n in the direction $\hat{x}_n$ is modeled by the following equation:

$$F_n = \begin{cases} -(K_n h_f + D_n \dot{h}_f) \cdot \hat{x}_n & h_f \leq 0 \\ 0 & else \end{cases} \quad (12)$$

In the shear direction of the wall surface, friction F_s in the direction $\hat{z}_n$ is modeled using a damper, and it can be expressed as:

$$F_s = \begin{cases} -D_s \dot{h}_f \cdot \hat{z}_n & h_f \leq 0 \\ 0 & else \end{cases} \quad (13)$$

IV. SIMULATION

A. Flip Phase: Impact and Upward-Flip in Simplified Model

To determine which coefficients (k_k and b_k) satisfy the condition $\frac{d\theta}{dt} = 0, \frac{d^b x}{dt} = 0$, and to probe the roles of k_k and b_k, the following simulations were conducted.

The initial parameters of the simplified model were given in advance – $m_c = 0.042$ kg, v_0=2 m/s, $\theta_0 = \frac{\pi}{3}$, L_0=0.15 m – according to the experimental platforms. The corresponding θ_{min}=0.574 was calculated according to Eq. (6). According to Eq. (4), the analytic expressions of k_k can be expressed as:

$$k_k = \frac{m_c v_0^2 - 2m_c g(L_0 cos\theta - {}^b x cos\theta - L_0 cos\theta_0) - 2\int_0^{t_b} b_k {}^b \dot{x}^2 dt}{{}^b x^2} \quad (14)$$

Assuming that the damping coefficient is infinitely small and takes a reasonable compression ${}^b x$, the spring stiffness k_k can be calculated using the above formula. To analyze the effect of compression on potential energy and taking ${}^b x = 0.1m$ (within the scope of L_0), the stiffness k_k=19.52 can be calculated according to Eq. (14). Because the spring has an influence on θ_{min} at the maximum altitude, the calculated k_k coefficient cannot actually satisfy the condition of the zero kinetic energy state. This error can be compensated by adjusting the overall stiffness and damping. According to the simulation, the model reaches its highest point faster than the spring reaches its maximum compression when k_k=19.52; therefore, the spring can be made to reach its maximum compression faster by appropriately increasing k_k. If k_k=20 and b_k=0, the condition of the zero kinetic energy state is satisfied. Using this approach, it is possible to obtain data from two other groups, which are both in the zero kinetic energy state, and to compare the coefficients of these three groups, as shown in Table IV.

It was found that different coefficients k_k and b_k caused different proportions of the gravitational and spring potential energies. When the initial kinetic energy is 0.084 J and the initial gravitational potential energy is 0.031 J, the data show that a higher b_k causes more energy to be consumed through damping, and it is dissipated as heat. If converted into more gravitational potential energy, the stored energy can be consumed by exerting the thrust of a propeller to perform negative work, but it requires
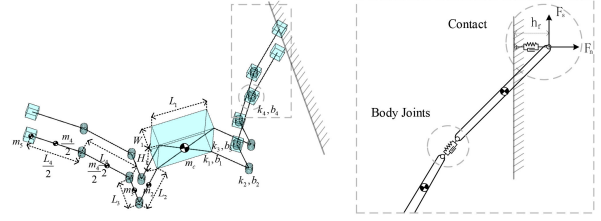

Fig. 5. Contact: Contact model between the adsorption part and the wall surface is modeled using an spring-damper as in a previous study [31]. Body Joints: Some joints need to realize elastic characteristic through impedance control.

more time and electric power consumption during falling. If this is converted into more spring potential energy, then the CoM does not flip upward too high, and the control of the downward swing requires less electric energy and time. Moreover, when the damper is too heavy, most of the energy is consumed, and only the remaining energy $\frac{m_c v_v^2}{2}$ is converted into gravitational potential energy and spring potential energy.

B. Flap Phase: Controlled Downward Swing in Simplified Model

During the downward swing, the PD controller is triggered by the rotational velocity, which generates controlled thrust, dissipates potential energy, and achieves smooth landing on the surfaces.

The propeller thrust F_t is a function of the gain k_d, with $k_p = 0.1$. In this study, k_p was set to a small value, causing the mass of the flying object to play the same role during the downward swing. Thus, the downward swing motion was adjusted by tuning k_d. As shown in Fig. 6, $k_d = 1.5$ was taken to illustrate this. The flying object begins falling at an angle $\theta \approx 41°$ at ① and reaches $\theta = 90°$ at ②, which corresponds to a normal rebound force of 0. Subsequently, the normal rebound force increases to a maximum at ③ and smoothly reaches $\theta = 180°$ at ④, achieving a stable landing state.

The simulation reveals that a larger k_d reduces both the normal rebound force F_n and the rotational velocity $\dot{\theta}$ during downward-swing, but it requires more time to land. Simulations revealed that the normal rebound force did not exceed 0.255 N.

The following conclusions are supported by the above simulation in the simplified model. Different groups of coefficients (in the zero kinetic energy state) result in different potential energy ratios. The potential energy accumulated by flipping up is consumed by the controlled thrust during the downward swing, which contributes to reducing the wall normal force and rotational velocity. Thus, a *flip-and-flap* strategy is proposed based on the above phased simulation in a simplified model.

C. Flip-and-Flap Dynamics Simulation in Multi-Links Model

The *flip-and-flap* strategy validation was performed during the entire process in a more complex simulation environment, consisting of several interacting submodels. In the following simulation, the performance of the pitch PD controller was mainly probed during downward swing under the selected coefficient of the extended leg.

The parameters were defined in Fig. 5 and Table III. The conditions in this simulation were v_0 =2 m/s, m_c=0.042 kg, m_2=0.005 kg, m_3=0.007 kg, m_4=0.012 kg, m_5=0.002 kg,
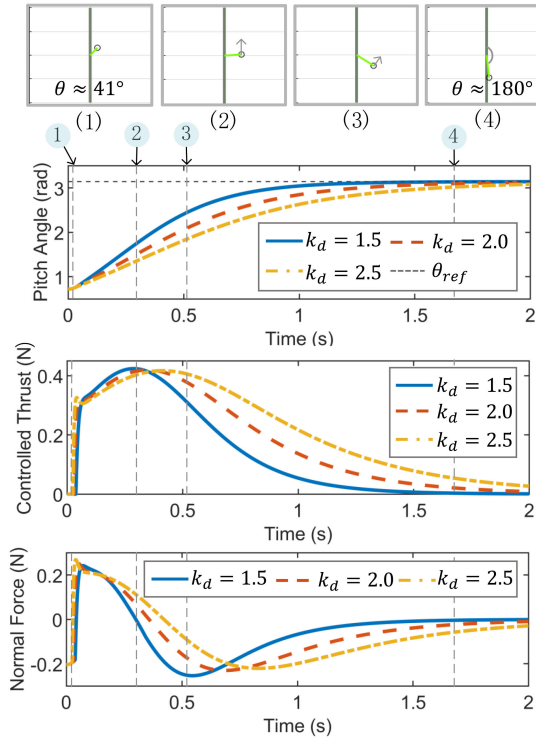
Fig. 6. (Top) Four simulated snapshots during downward-swing. (Middle 1) The PD controller performance in pitching the object by downward swing into the stable landing state. (Middle 2) The simulation signal of controlled thrust F_t. (Bottom) The normal force F_n as the flying object downward swings to its stable landing state.

L_1=0.08 m, W_1=0.08 m, H_1=0.03 m, L_2=0.05 m, L_3=0.04 m, L_4=0.15 m, K_n=2.0e4, D_n=1.0e0, D_s=2.7e1, k_i=[7.0e1, 7.0e1, 5.0e1, 5.0e1], b_i=[6.75, 6.75, 25.5, 15.75], and $i \in$[1,2,3,4].

In the following simulation, the initial pitch angle of the flying object is $\theta = -30°$ and smoothly reaches $\theta = 45°$ under the control strategy, as shown in Fig. 7 (top). Except for the contact point with the adsorption capacity, the contact forces at other points are neglected in this model. The propeller thrust is a mapping related to the k_p and k_d parameters in the pitch controller. It is inferred that k_p is small because gravity plays the same role as k_p during the downward-swing process, and k_p is set to 0.1. In addition, the controller output is normalized and multiplied by the maximum thrust to obtain a new thrust. When the flying object triggers the optimization condition, the torque $\tau = 0.5L_b \times F_t$, which is equivalent to turning on the rear propeller.

Fig. 7 (middle) reveals that a higher k_d can reduce the pitch angular velocity and control the object so that it lands more stably on the wall, but it takes more time. The multilink model is somewhat different from the simplified model because it is not just a single swing up and down. The multilink motion is more complex because it consists of several interacting submodels, such as the body joint model. If one takes out the simple falling phase from ⑤ to ⑧ – the same scenario as the simplified model – the simulation shows that the strategy contributes to the 0.5 N reduction of normal force at ⑥, shown in Fig. 7 (bottom).

Thus, the above conclusion in the simplified model was further corroborated in the simulation of the entire process in the multilink model. In summary, to achieve landing without deceleration,
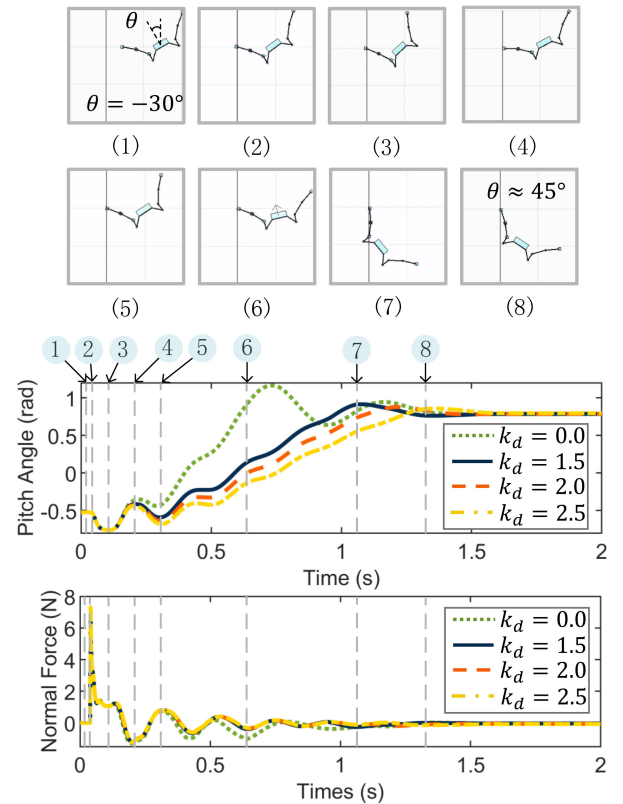

Fig. 7. (Top) Eight simulated snapshots during perching. (Middle) The controller performance in pitching the flying object. The movement of the snapshots is: in a horizontal flight at ①, collision occurs at ②, elastic structure is compressed and starts to flip from ② to ③, pulling off the wall occurs from ③ to ④, dragging back to the wall occurs from ④ to ⑤, controlled downward-swing happens from ⑤ to ⑧, maximum F_n is reached at ⑥, and stable landing occurs at ⑧. (Bottom) Normal force during the entire process.

energy can be converted by flipping up and compressing the extended leg during the flip-upward phase. Specifically, the kinetic energy is converted into gravitational potential energy through an upward flip. As the elastic extended leg is compressed, the spring potential energy is stored but not released at the moment of rebound. In a controlled downward swing, the thrust of the propeller serves two purposes. The first is to consume the stored gravitational potential energy by performing negative work. The second is to resist the gravitational moment, reducing the rotational velocity of the pitch angle. Eventually, the flying object lands on the surface and reaches a stable landing state.

V. EXPERIMENTAL VALIDATION

To confirm that the proposed *flip-and-flap* strategy can accurately help the flying object perch stably on a wall surface, experiments comparing the two landing methods were performed on the selected flying object (Crazyflie with the customized extended-leg mechanism). The basic one shuts off the motors when the IMU detects impact on the surface, and it only applies a flip operation. The other one applies the *flip-and-flap* strategy, applying flip operation and activating flap operation when the optimization condition is triggered.

Both methods were used at the vertical wall surface ($\alpha = 0°$) and negative inclined wall surface ($\alpha = -30°$). As shown

(a)Unsuccessful landing on vertical surface(α=0, v_0 =3.4m/s), only with flip operation.

(b)Successful landing on vertical surface (α=0, v_0 =3.4m/s), with flip-and-flap strategy.

(c)Unsuccessful landing on inclined surface (α=-30°, v_0 =2.8m/s), only with flip operation.

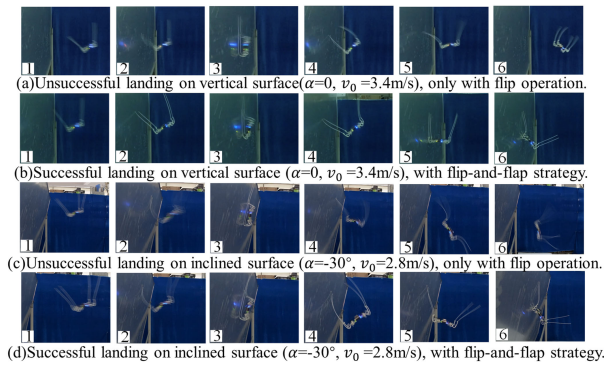(d)Successful landing on inclined surface (α=-30°, v_0 =2.8m/s), with flip-and-flap strategy.

Fig. 8. Back-to-back perching experiment (left to right, top to bottom). (a) and (b) experimental initial conditions before touchdown: pitch angle was set to $30°$, the thrust parameter was set to 52 000 and the flight distance was set to 2.4 m. (c) and (d) experimental initial conditions before touchdown: pitch angle was set to $25°$, the thrust parameter was set to 50 000 and the flight distance was set to 1.8 m.

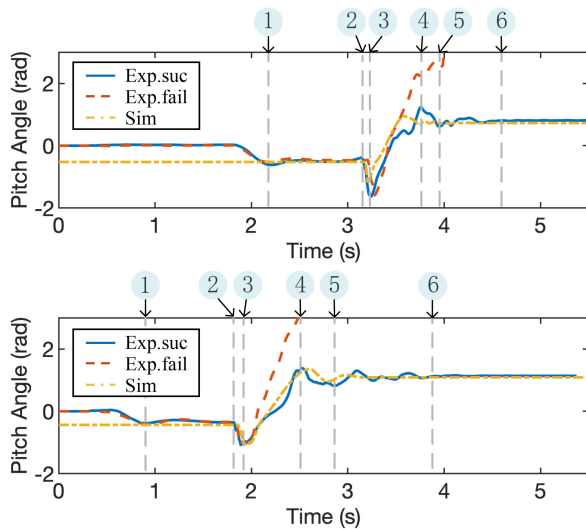Fig. 9. Experimental pitch angle data in successful and unsuccessful trials, and simulation data of maximum landing velocity. (Top) α=0°, (Bottom) α=−30°. The key timing is as follows, flying to the surface during ①, collision and starting to flip up occurs at ②, falling begins at ③, controlled downward-swing happens during ③-⑤, and landing stably occurs at ⑥.

in Fig. 8, the *flip-and-flap* strategy was applied to perch on the wall successfully; only the flip operation can cause failure. Fig. 8 b shows successive snapshots of a successful flip-and-flap operation on a vertical surface. As shown in the second panel of the figure, the collision occurs, and the extended legs start to interact with the wall as it is pressurized. From the second panel to third panel, as the entire object flips up, the kinetic energy of the flying object is converted into gravitational and spring potential energy. In the fourth panel, the flip phase terminates, and the flap phase begins. In the fifth and sixth panels, the flying object starts to fall under controlled thrust. To look more closely at the differences in movements, a comparison of the pitch angles between the two methods is shown in Fig. 9. In addition, a comparison of the pitch angle between the experiment and simulation is also shown in Fig. 9.

For the vertical surface (as shown in Fig. 8 a), when the initial normal velocity exceeded 1.6 m/s, landing on the wall

surface did not occur with only the flip operation. When the proposed flip-and-flap strategy was applied (as shown in Fig. 8 b), the flying object successfully perched in 15/20 trials with a maximum normal velocity of approximately 3.4 m/s. For the inclined surface (as shown in Fig. 8 c), when the initial normal velocity exceeded 1.4 m/s, landing on the wall surface was unsuccessful with only the flip operation. When the flip-and-flap strategy was applied (as shown in Fig. 8 d), the flying object successfully perched in 12/20 trials with a maximum normal velocity of approximately 2.8 m/s.

The energy consumption during landing occurred mainly in the downward-swinging process. For vertical-surface landing, the duration of the thrust opening was approximately 1 s. The energy consumption was estimated based on the power corresponding to the peak thrust, which was approximately 12 J. For inclined-surface landing, the duration of thrust opening was approximately 0.39 s, and the corresponding power was 4.6 J.

The experimental results verify that the proposed *flip-and-flap* strategy enables the quadrotor to land on vertical and inclined surfaces without prior deceleration. When the extended leg is utilized, the kinetic energy can be effectively converted into spring and gravitational potential energy. Then, the potential energy is consumed by the controlled thrust during downward-swing movement.

There were some trials in which the flying object failed to land. It is possible that the main reason is that the lithium battery charge of the aircraft was too high a voltage when it was full, causing the aircraft to fly faster than expected.

The maximum speed allowed for different wall surfaces was obtained by gradually increasing the speed in the experiment and repeated testing. The upper limit of the maximum speed was influenced by a combination of factors, including the stiffness and length of the extended leg, adsorption force, and angle at which upturning was allowed. The maximum landing speed for a vertical surface was faster than that for inclined surfaces. The main reason for the difference in maximum speed is probably the difference in the angle allowed for flipping up. For the negatively inclined surface, the angle allowed was only $60°$, whereas, for the vertical surface, it was $90°$. In other words, on a negative inclined wall, the potential energy converted by the quadrotor through upward flipping was limited. As a result, the quadrotor could not decelerate completely, leading to a secondary collision with the wall. Proper optimization of the stiffness and length of the elastic foot may be beneficial for increasing the potential energy that can be transformed during upturning, thus increasing the allowable landing speed. However, the above method is constrained when it comes to increasing the allowed maximum velocity because it must also consider whether the thrust during the swing is sufficient to consume the potential energy. Further study of the optimization problem is planned.

Fig. 9 indicates that the trend of the angle change in the simulation and experiment is consistent. The quadrotor flipped upward after impact with the wall and then started to swing downward under the effect of gravity and thrust. The maximum upturn angle of the simulation was smaller than that in the experiment. In addition, the speed of downward swinging and the maximum overshoot of the pitch angle were smaller than those in the experiment. This might be caused by the difference between the multilink model and the actual tie, which is a continuous elastomer. Nevertheless, the results show that the model guides the parameter tuning of the landing strategy to some extent.

In this study, the focus was on imitation of behavior rather than the mass or body length ratio. A housefly was not actually used as a scale factor. The weight of a housefly is 12 mg, whereas the flying object in this work was 42 g. The ratio of the front legs to the body of the fly is approximately 1:1.3 [4], while the ratio of the robot was approximately 1:0.34. The extended leg was longer than the foreleg of the insect. The landing strategy has the potential to be applied to other micro aerial vehicles with various masses or sizes. Some qualitative conclusions are that, as the torso mass increases, the leg length must follow to ensure that the gravitational potential energy generated during the upward swing is sufficient to offset the kinetic energy. However, for large-scale vehicles, this strategy may not be realistic because the swinging foot becomes too long. In addition, such coefficients as maximum allowable thrust, stiffness, and damping play a regulatory role; however, they are not independently decoupled but are rather mutually constrained. As a result, the relationship between the corresponding parameters related to the scale factor should be further studied.

VI. CONCLUSION

A new biomimetic *flip-and-flap* strategy that enables a high-speed flying object to perch on negatively inclined surfaces without speed reduction before touchdown is proposed. This is achieved by two key strategies: one is that the flipping operation was completed with the assistance of the extended leg to convert energy, and the other is performing flapping motion through feedback-controlled thrust during the downward swing, reducing the total energy of the system. The *flip-and-flap* strategy was demonstrated by performing a set of simulations and experiments on the surface-landing task. The experimental results show that the *flip-and-flap* strategy works well not only on vertical walls but also on negatively inclined surfaces, making landing without deceleration possible.

The contribution of this study is a new landing method that does not require deceleration and can adapt to inclined walls to some extent. Without deceleration, the flying object does not require human remote assistance or reliance on precise sensors to detect distances and plan landing. This is a significant difference from most landing methods that require deceleration in advance. This landing method complements other previous wall-landing methods and helps improve the success rate of wall-surface landings in environments with poor visual conditions.

REFERENCES

[1] W. G. Hyzer, "Flight behavior of a fly alighting on a ceiling," *Science*, vol. 137, no. 3530, pp. 609–610, 1962.

[2] S. Balebail, S. K. Raja, and S. P. Sane, "Landing maneuvers of house-flies on vertical and inverted surfaces," *PloS One*, vol. 14, no. 8, 2019, Art. no. e0219861.

[3] M. Kovac, "Learning from nature how to land aerial robots," *Science*, vol. 352, no. 6288, pp. 895–896, 2016.

[4] C. G. Hewitt, "The structure, development, and bionomics of the house-fly, musca domestica, linn: Part III—The bionomics, allies, parasites, and the relations of M. domeestica to human disease," Q. *J. Microsc. Sci.*, vol. 2, no. 215, pp. 347–414, 1909.

[5] J. Attila Bergou *et al.*, "Falling with style: Bats perform complex aerial rotations by adjusting wing inertia," *PloS Biol.*, vol. 13, no. 11, 2015, Art. no. e1002297.

[6] A. M. Adams, K. Davis, and M. Smotherman, "Suppression of emission rates improves sonar performance by flying bats," *Sci. Rep.*, vol. 7, no. 1, pp. 1–9, 2017.

[7] A. Ramezani, S. J. Chung, and S. Hutchinson, "A biomimetic robotic platform to study flight specializations of bats," *Sci. Robot.* vol. 2, no. 3, 2017, Art. no. eaal2505.

[8] W. R. Roderick, M. R. Cutkosky, and D. Lentink, "Touchdown to take-off: At the interface of flight and surface locomotion," *Interface Focus*, vol. 7, no. 1, 2017, Art. no. 20160094.

[9] D. Mehanovic, D. Rancourt, and A. L. Desbiens, "Fast and efficient aerial climbing of vertical surfaces using fixed-wing UAVs," *IEEE Robot. Automat. Lett.*, vol. 4, no. 1, pp. 97–104, Jan. 2019.

[10] D. Mellinger, M. Shomin, and V. Kumar, "Control of quadrotors for robust perching and landing," in *Proc. Int. Powered Lift Conf.*, 2010, pp. 205–225.

[11] A. Lussier Desbiens, A. Asbeck, and M. R. Cutkosky, "Landing, perching and taking off from vertical surfaces," *Int. J. Robot. Res.*, vol. 30, no. 3, pp. 355–370, 2011.

[12] P. Chirarattananon, K. Y. Ma, and R. J. Wood, "Fly on the wall," in *Proc. IEEE RAS/EMBS Int. Conf. Biomed. Robot. Biomechatronics, Sao Paulo, Brazil*, 2014, pp. 1001–1008.

[13] M. Cutkowsky and A. Desbiens, "Bio-inspired perching and crawling air vehicles," White paper, Stanford Univ., pp. 1–21, 2008.

[14] H. Jiang *et al.*, "Modeling the dynamics of perching with opposed-grip mechanisms," in *Proc. IEEE Int. Conf. Robot. Automat.*, 2014, pp. 3102–3108.

[15] H. Jiang *et al.*, "Perching failure detection and recovery with on-board sensing," in *Proc. IEEE Int. Conf. Intell. Robots Syst.*, 2015, pp. 1264–1270.

[16] D. Mehanovic, J. Bass, T. Courteau, D. Rancourt, and A. L. Desbiens, "Autonomous Thrust-Assisted Perching of a Fixed-Wing UAV on Vertical Surfaces," in *Proc. Conf. Biomimetic Biohybrid Syst.*, 2017, pp. 302–314.

[17] L. Daler, A. Klaptocz, A. Briod, M. Sitti, and D. Floreano, "A perching mechanism for flying robots using a fibre-based adhesive," *IEEE Int. Conf. Robot. Automat.*, 2013, pp. 4433–4438.

[18] A. Kalantari, K. Mahajan, D. Ruffatto, and M. Spenko, "Autonomous perching and take-off on vertical walls for a quadrotor micro air vehicle," in *IEEE Int. Conf. Robot. Automat.*, 2015, pp. 4669–4674.

[19] H. W. Wopereis, T. D. van der Molen, T. H. Post, S. Stramigioli, and M. Fumagalli, "Mechanism for perching on smooth surfaces using aerial impacts," *IEEE SSRR*, 2016, pp. 154–159.

[20] M. A. Graule *et al.*, "Perching and takeoff of a robotic insect on overhangs using switchable electrostatic adhesion," *Science*, vol. 352, no. 6288, pp. 978–982, 2016.

[21] M. T. Pope *et al.*, "A multimodal robot for perching and climbing on vertical outdoor surfaces," *IEEE Trans. Robot.*, vol. 33, no. 1, pp. 38–48, Feb. 2017.

[22] H. Tsukagoshi, M. Watanabe, T. Hamada, D. Ashlih, and R. Iizuka, "Aerial manipulator with perching and door-opening capability," *IEEE Int. Conf. Robot. Automat.*, 2015, pp. 4663–4668.

[23] J. Dougherty, D. Lee,, and T. Lee, "Laser-based guidance of a quadrotor uav for precise landing on an inclined surface," in *Proc. Amer. Control Conf.*, 2014, pp. 1210–1215.

[24] J. Thomas *et al.*, "Aggressive flight with quadrotors for perching on inclined surfaces," *J. Mech. Robot*, vol. 8, no. 5, 2016, Art. no. 051007.

[25] F. von Frankenberg, S. B. Nokleby, "Inclined landing testing of an omni-directional unmanned aerial vehicle," *Trans. Can. Soc. Mech. Eng.*, vol. 42, no. 1, pp. 61–70, 2018.

[26] J. Bass, and A. L. Desbiens, "Improving multirotor landing performance on inclined surfaces using reverse thrust," *IEEE Robot. Automat. Lett.*, vol. 5, no. 4, pp. 5850–5857, Oct. 2020.

[27] W. Shyy, M. Berg, and D. Ljungqvist, "Flapping and flexible wings for biological and micro air vehicles," *Progress Aerosp. Sci.*, vol. 35, no. 5, pp. 455–505, 1999.

[28] B. Landry, "Planning and control for quadrotor flight through cluttered environments,"M.S. thesis, Massachusetts Inst. Technol., Cambridge, MA, USA, 2015.

[29] Bitcraze, "Crazyflie nano quadcopter," Accessed: Mar. 1, 2021. [Online]. Available: https://www.bitcraze.io/products/old-products/crazyflie-2-0//

[30] M. W. Walker and D. E. Orin, "Efficient dynamics computer simulation of robotic mechanisms," *J. Dyn. Syst. Meas. Control*, vol. 104, pp. 205–211, 1982.

[31] K. L. Johnson, "*Contact Mechanics*," Cambridge, U.K.: Cambridge Univ. Press, 1987, pp. 1–445.

[32] C. Evangelista, P. Kraft, M. Dacke, J. Reinhard, and M. V. Srinivasan, "The moment before touchdown: Landing manoeuvres of the honeybee apis mellifera," *J. Exp. Biol.*, vol. 213, no. 2, pp. 262–270, 2010.

[33] R. J. Bomphrey, T. Nakata, N. Phillips, and S. M. Walker, "Smart wing rotation and trailing-edge vortices enable high frequency mosquito flight," *Nature*, vol. 544, no. 7648, pp. 92–95, 2017.